arXiv:nucl-th/0101030v2 25 Jan 2001

# Four-body DWBA calculations of the Coulomb breakup of $^{6}$He

R. Chatterjee [a], P. Banerjee [b], R. Shyam [a,c]

[a] *Theory Group, Saha Institute of Nuclear Physics, 1/AF Bidhan Nagar, Calcutta - 700 064, INDIA.*

[b] *Physics Group, Variable Energy Cyclotron Centre, 1/AF Bidhan Nagar, Calcutta - 700 064, INDIA.*

[c] *National Superconducting Cyclotron Laboratory, Michigan State University, East Lansing, MI 48824, U.S.A.*

---

## Abstract

We investigate the Coulomb breakup of the two-neutron halo nucleus $^{6}$He by extending the framework of the finite range post form distorted wave Born approximation theory introduced earlier for the description of the breakup of one-neutron halo nuclei. The model can use the realistic three-body wave function for the $^{6}$He ground state. Calculations have been performed for energy, total and parallel momentum distributions of $^{4}$He fragment. The two-body $^{4}$He-neutron and neutron-neutron correlations have also been calculated. Our results are compared with those of an adiabatic model of the Coulomb breakup reactions. The two theories lead to almost identical results. Comparisons are also made with the available experimental data. It is found that the pure Coulomb breakup can describe the bulk of the data taken at below grazing angles. However, a rigorous description of all the available data requires the consideration of the nuclear breakup effects.
PACS numbers: 21.60.-n, 24.50.+g, 25.60.-t, 25.60.Gc

*Key words:* Coulomb breakup of $^{6}$He, two-neutron halo nucleus, post form DWBA with finite range effects.

---

## 1 Introduction

Several nuclei near the drip lines have been found to have properties which are strikingly different from those of their stable counterparts. These nuclei have a halo structure in their ground states in which loosely bound valence nucleon(s) has (have) a large spatial extension with respect to the respective core [1–5]. The two-neutron halo nuclei, of which $^{6}$He is a prominent example, have attracted a lot of attention. These are Borromean three-body systems, where all the two-body subsystems are unbound [3,6]. Clearly, the interaction of valence neutrons is vital for the stability of the two-neutron halo nuclei. They provide interesting examples of the three-body problem in the limit of very weak binding [7], and the three-body methods (within both Faddeev and cluster type approaches) have been extensively applied to study them [3,8–19]. Other approaches like non-relativistic [20] and relativistic [21,22] mean field models and many-body calculations [23] have also been used to investigate the structure of such nuclei.

Breakup reactions, in which the valence neutrons are removed from the core in the interaction of halo nuclei with stable targets, provide detailed information on their structures [24]. The study of the breakup reaction of $^6$He is interesting due to several reasons. It leads to the excitation of the continuum of this nucleus, which has received much attention recently due to the experimental discovery [25] of the soft dipole resonance (SDR), signifying the dipole oscillation between the core cluster and the valence neutrons. Although the SDR was predicted long ago [4,9], properties of this resonance measured in Ref. [25] are at variance with those predicted by the detailed three-body calculations [16]. The breakup reaction of this nucleus gives access to the study of the neutron-neutron ($n$-$n$) and neutron-alpha particle ($n$-$^4$He) correlations, which are important because they provide a critical test of the dineutron model, in which the halo neutrons were treated as a point like "dineutron" cluster orbiting the core. This model has been used in earlier theoretical studies, both semiclassical [26] and quantum mechanical [27,28], of the breakup of the two-neutron halo nuclei. Furthermore, the study of the neutron-$^4$He correlation is expected to constrain the neutron-$^4$He interaction used in the three-body calculations of the $^6$He ground state. The study of the total and longitudinal momentum distributions of the charged fragment is expected to yield information on the matter radii of the halo. The breakup of $^6$He is also important from the viewpoint of astrophysics as it can be used [29] to extract the rate of the $^4$He$(2n,\gamma)^6$He$(2n,\gamma)^8$He reactions which could be a possible route for bridging the gap at the mass number, $A = 5$ and 8.

Several calculations of the nuclear and Coulomb breakup [30–33] of $^6$He, based on a model which uses a sudden approximation [34,35], have been reported recently. Calculations of the nuclear breakup of $^6$He within the approximate eikonal model is reported in Ref. [36]. Due to the nature of the approximations involved in these models, their applicability is limited to reactions at higher beam energies ($>$ 200 MeV/nucleon). Moreover, they have been applied to describe only a selected set of observables. In the distorted wave Born approximation (DWBA) calculations of the breakup of $^6$He reported in [37], the interaction appearing in the kernel of the prior DWBA T-matrix has been evaluated in the impulse approximation which limits its applicability to higher beam energies.

In this paper, we calculate the Coulomb breakup of $^6$He treating the final state as a four-body system. Our formalism uses the framework of the post form distorted wave Born approximation which is an extension of the theory developed earlier [24] to describe the breakup of one-neutron halo nuclei. Finite range of the interaction between projectile constituents is treated by making an effective local momentum approximation (ELMA) on the distorted wave of the charged core in the final channel. It was shown in Ref. [24] that this approximation is well satisfied for the breakup of one-neutron halo nuclei. Furthermore, this gave results [24] which were similar to those obtained within an adiabatic model (AD) [38] of Coulomb breakup reactions. This theory allows the use of a realistic three-body wave function for the projectile ground state and can be applied to breakup reactions with beam energies ranging from below the Coulomb barrier to higher values up to which the non-relativistic treatment is valid. We have used our theory to analyze almost all types of the breakup observables measured in the reaction of $^6$He on heavy target nuclei. We compare our results with those of the AD and dineutron models.

This paper is organized in the following way. Our formalism is presented in the next section. The structure models of $^6$He are discussed in section 3. The results of our calculations and discussions are presented in section 4. A summary and the conclusions of our work are given in section 5.

## 2 Formalism

We consider the breakup reaction $a + t \to b + n_1 + n_2 + t$, where the projectile $a$ breaks up into fragment $b$ (the charged core) and the two valence neutrons ($n_1$ and $n_2$) in the Coulomb field of the heavy target $t$. We consider only the elastic breakup mode in which the target nucleus remains in its ground state during the breakup process. The system of coordinates is shown in Fig. 1. The position vectors satisfy the relations

$$\mathbf{r}_b = \mathbf{r}_i - \alpha\mathbf{R}, \qquad \alpha = \frac{2m_n}{2m_n + m_b}, \tag{1}$$

$$\mathbf{r}_c = \beta\mathbf{r}_i + \delta\mathbf{R}, \qquad \beta = \frac{m_t}{m_b + m_t}, \qquad \delta = (1 - \alpha\beta). \tag{2}$$

The post form $T$ - matrix for this case is given by

$$T = \langle \chi^{(-)}_{b-t}(\mathbf{k}_b, \mathbf{r}_b)\phi_b(\xi_b)\chi^{(-)}_{c-bt}(\mathbf{k}_c, \mathbf{r}_c)\phi_{n_1n_2}(\mathbf{k}, \mathbf{r}, \xi_{n_1n_2})|V(\mathbf{R}, \mathbf{r})| \\ \times \Psi^{(+)}_a(\xi_a, \mathbf{R}, \mathbf{r}, \mathbf{r}_i)\rangle, \tag{3}$$

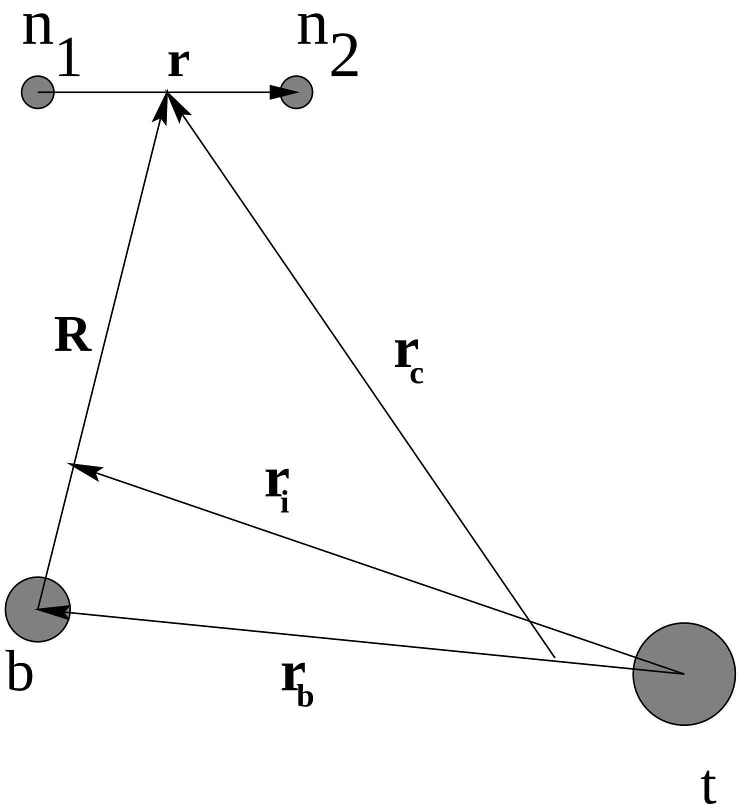

Fig. 1. The four – body coordinate system. $n_1, n_2$ are the valence neutrons. $b$ and $t$ represent the charged core and the target respectively.

where $c$ represents the c.m. of the $n_1 - n_2$ system. $\chi^{(-)}_{b-t}$ is the Coulomb distorted wave describing the motion of the charged core ($b$) with respect to target $t$ with incoming wave boundary condition and $\chi^{(-)}_{c-bt}$ describes the c.m. motion of the valence neutrons with respect to the c.m. of the $b$-$t$ system. $\phi$'s are the internal state wave functions of the concerned particles with $\xi$'s being the internal coordinates. $\mathbf{k}_b$ and $\mathbf{k}_c$ are the Jacobi wave vectors conjugate to $\mathbf{r}_b$ and $\mathbf{r}_c$ respectively. $\Psi^{(+)}_a(\xi_a, \mathbf{R}, \mathbf{r}, \mathbf{r}_i)$ represents the exact four-body scattering wave function of the projectile with an outgoing wave boundary condition. $\mathbf{k}_a$ is the wave vector associated with it. $V(\mathbf{R}, \mathbf{r})$ is the sum of the two-body interactions between the projectile constituents, given by

$$V(\mathbf{R}, \mathbf{r}) = V_{n_1 n_2}(\mathbf{r}) + V_{bn_1}(\mathbf{R} - \mathbf{r}/2) + V_{bn_2}(\mathbf{R} + \mathbf{r}/2). \qquad (4)$$

### *2.1 Transition amplitude within the finite range distorted wave Born approximation (FRDWBA)*

In DWBA theory the breakup states are assumed to be weakly coupled and hence this coupling is treated only up to the first order. Thus we can write

$$\Psi_a^{(+)}(\xi_a, \mathbf{R}, \mathbf{r}, \mathbf{r}_i) = \phi_a(\xi_a, \mathbf{R}, \mathbf{r})\chi_{a-t}^{(+)}(\mathbf{k}_a, \mathbf{r}_i), \tag{5}$$

where $\phi_a(\xi_a, \mathbf{R}, \mathbf{r})$ represents the (three-body) bound state wave function of the projectile and $\chi_{a-t}^{(+)}(\mathbf{k}_a, \mathbf{r}_i)$ is the Coulomb distorted scattering wave describing the relative motion of the c.m. of the projectile with respect to the target with outgoing wave boundary condition. Substituting Eq. (5) into Eq. (3) and writing the latter in the integral form we get,

$$\begin{aligned} T^{DWBA} = &\int\int\int\int d\xi d\mathbf{R} d\mathbf{r} d\mathbf{r}_i \chi_{b-t}^{(-)*}(\mathbf{k}_b, \mathbf{r}_b)\phi_b^*(\xi_b)\chi_{c-bt}^{(-)*}(\mathbf{k}_c, \mathbf{r}_c) \\ &\times \phi_{n_1 n_2}^*(\mathbf{k}, \mathbf{r}, \xi_{n_1 n_2}) V(\mathbf{R}, \mathbf{r})\phi_a(\xi_a, \mathbf{R}, \mathbf{r})\chi_{a-t}^{(+)}(\mathbf{k}_a, \mathbf{r}_i). \end{aligned} \tag{6}$$

We introduce the finite range effects in DWBA by an effective local momentum approximation by writing the distorted wave in the final channel as [24]

$$\chi_b^{(-)*}(\mathbf{k}_b, \mathbf{r}_b) = e^{i\alpha \mathbf{K}\cdot\mathbf{R}}\chi_b^{(+)}(-\mathbf{k}_b, \mathbf{r}_i), \tag{7}$$

where $\mathbf{K}$ is an effective local momentum whose direction is taken to be the same as that of the asymptotic momentum $\mathbf{k}_b$, since the calculated cross sections are almost independent of this quantity, as is shown in Appendix A. The magnitude of $\mathbf{K}$ is given by

$$K(R_d) = \sqrt{\frac{2\mu_{b-t}}{\hbar^2}(E - V(R_d))}. \tag{8}$$

In Eq. (8) $\mu_{b-t}$ is the reduced mass of the $b$-$t$ system, $E$ is the energy of particle $b$ relative to the target in the c.m. system and $V(R_d)$ is the Coulomb potential between $b$ and the target at a distance $R_d$. Thus, the magnitude of $\mathbf{K}$ is evaluated at a separation $R_d$ (taken to be 10 fm in all the numerical calculations shown in the next section), which is held fixed for all the values of $r$. We refer to Appendix A for further discussions of the validity of this approximation for the reactions studied in this paper.

In Eq. (6), the Coulomb distorted waves are given by

$$\chi_{a-t}^{(+)}(\mathbf{k}_a, \mathbf{r}_i) = e^{-\pi\eta_a/2}\Gamma(1 + i\eta_a)e^{i\mathbf{k}_a\cdot\mathbf{r}_i}{}_1F_1(-i\eta_a, 1, i(k_a r_i - \mathbf{k}_a\cdot\mathbf{r}_i)), \tag{9}$$

$$\begin{aligned} \chi_{b-t}^{(-)*}(\mathbf{k}_b, \mathbf{r}_b) = &e^{i\alpha\mathbf{K}\cdot\mathbf{R}}e^{-\pi\eta_b/2}\Gamma(1 + i\eta_b)e^{-i\mathbf{k}_b\cdot\mathbf{r}_i} \\ &\times {}_1F_1(-i\eta_b, 1, i(k_b r_i + \mathbf{k}_b\cdot\mathbf{r}_i)). \end{aligned} \tag{10}$$

For pure Coulomb breakup, the interactions between two uncharged valence particles as well as between their c.m. and that of the $b$-$t$ system are zero. Hence we take plane waves for the $c$-$bt$ and $n_1$-$n_2$ relative motions:

$$\chi^{(-)*}_{c-bt}(\mathbf{k}_c,\mathbf{r}_c) = e^{-i\beta\mathbf{k}_c\cdot\mathbf{r}_i}e^{-i\delta\mathbf{k}_c\cdot\mathbf{R}}, \tag{11}$$

$$\phi^{*}_{n_1n_2}(\mathbf{k},\mathbf{r},\xi_{12}) = e^{-i\mathbf{k}\cdot\mathbf{r}}\phi^{*}_{n_1n_2}(\xi_{12}). \tag{12}$$

Substituting Eqs. (9-12) into Eq. (6) we get,

$$\begin{aligned} T^{FRDWBA} &= e^{-\pi(\eta_a+\eta_b)/2}\Gamma(1+i\eta_a)\Gamma(1+i\eta_b) \\ &\times\Big[\int d\mathbf{r}_i e^{i(\mathbf{k}_a-\mathbf{k}_b-\beta\mathbf{k}_c)\cdot\mathbf{r}_i}\,{}_1F_1(-i\eta_a,1,i(k_ar_i-\mathbf{k}_a\cdot\mathbf{r}_i)) \\ &\times\,{}_1F_1(-i\eta_b,1,i(k_br_i+\mathbf{k}_b\cdot\mathbf{r}_i))\Big] \\ &\times\Big[\int d\mathbf{r}d\mathbf{R}d\xi e^{-i(\delta\mathbf{k}_c-\alpha\mathbf{K})\cdot\mathbf{R}}e^{-i\mathbf{k}\cdot\mathbf{r}}\phi^{*}_b(\xi_b)\phi^{*}_{n_1n_2}(\xi_{12})V(\mathbf{R},\mathbf{r}) \\ &\times\,\phi_a(\xi_a,\mathbf{R},\mathbf{r})\Big]. \end{aligned} \tag{13}$$

In Eq. (13), the first integral is associated with the dynamics of the reaction which can be expressed analytically in terms of the Bremsstrahlung integral [39]. The second one (to be expressed as $I_f^{FRDWBA}$) contains the information about the structure of the projectile and is known as the form factor. Defining $\delta\mathbf{k_c}-\alpha\mathbf{K}=\mathbf{k_1}$, we can write

$$\begin{aligned} I_f^{FRDWBA} &= \int d\mathbf{r}d\mathbf{R}e^{-i\mathbf{k_1}\cdot\mathbf{R}}e^{-i\mathbf{k}\cdot\mathbf{r}}\Big[\int d\xi\phi^{*}_b(\xi_b)\phi^{*}_{n_1n_2}(\xi_{12})V(\mathbf{R},\mathbf{r}) \\ &\times\,\phi_a(\xi_a,\mathbf{R},\mathbf{r})\Big]. \end{aligned} \tag{14}$$

The function $\Phi_a(\xi_a,\mathbf{R},\mathbf{r}) = V(\mathbf{R},\mathbf{r})\phi_a(\xi_a,\mathbf{R},\mathbf{r})$ has the following representation in configuration space [40,41]:

$$\sum_{l\lambda LS}\Phi_{l\lambda LS}(R,r)[[Y^l_m(\hat{\mathbf{r}})\otimes Y^\lambda_\mu(\hat{\mathbf{R}})]_L\otimes\chi_S]_{JM}. \tag{15}$$

In Eq. (15), the relative orbital angular momentum $\lambda$ between the core and c.m. of the two neutrons is coupled with the relative orbital angular momentum $l$ between the neutrons to give $L$, which, in turn, is coupled with the total intrinsic spin $S$ of the two valence neutrons to give the resultant total angular momentum $J$ of the projectile with projection $M$. For $^6$He, $J=M=0$.

Hence

$$\begin{aligned} &\int d\mathbf{r}d\mathbf{R}e^{-i(\delta\mathbf{k}_c-\alpha\mathbf{K})\cdot\mathbf{R}}e^{-i\mathbf{k}\cdot\mathbf{r}}V(\mathbf{R},\mathbf{r})\phi_a(\xi_a,\mathbf{R},\mathbf{r}) \\ &= 4\pi\sum_{l\lambda LS}(-i)^{l+\lambda}\Phi_{l\lambda LS}(k,k_1)[[Y^l_m(\hat{\mathbf{k}})\otimes Y^\lambda_\mu(\hat{\mathbf{k}}_1)]_L\otimes\chi_S]_{00}, \end{aligned} \tag{16}$$

where

$$\Phi_{l\lambda LS}(k,k_1) = 4\pi\int r^2dr\int R^2dRj_l(kr)j_\lambda(k_1R)\Phi_{l\lambda LS}(R,r). \tag{17}$$

The modulus square of $I_f^{FRDWBA}$ is given by

$$|I_f^{FRDWBA}|^2 = (4\pi)^2 \sum_{ll'\lambda\lambda' L\Lambda} (-)^{L+\Lambda} \Phi_{l\lambda LL}(k,k_1)\Phi_{l'\lambda' LL}(k,k_1) P_\Lambda(\cos\Theta)$$

$$\times \hat{l}\hat{l}'\hat{\lambda}\hat{\lambda}'\hat{\Lambda}^2 W(l\lambda l'\lambda'; L\Lambda) \begin{pmatrix} l & l' & \Lambda \\ 0 & 0 & 0 \end{pmatrix} \begin{pmatrix} \lambda & \lambda' & \Lambda \\ 0 & 0 & 0 \end{pmatrix}, \tag{18}$$

where $\Theta$ is the angle between vectors $\mathbf{k}_1$ and $\mathbf{k}$, and $\hat{n} = \sqrt{2n+1}$.

The dominant angular momentum configurations of $^6$He contributing to Eq. (18) are $\Phi_{0000}(k,k_1)$ and $\Phi_{1111}(k,k_1)$ (with probabilities of $\approx 0.84$ and $\approx 0.11$, respectively). Thus we have [40]

$$|I_f^{FRDWBA}|^2 = \Phi^2_{0000}(k,k_1) + \Phi^2_{1111}(k,k_1) - \Phi^2_{1111}(k,k_1) P_2(\cos\Theta). \tag{19}$$

The differential cross section for the breakup process is given by

$$\frac{d^5\sigma}{dE_b d\Omega_b dE_{n_1} d\Omega_{n_1} d\Omega_{n_2}} = \frac{2\pi}{\hbar v_a} \rho(E_b, \Omega_b, E_{n_1}, \Omega_{n_1}, \Omega_{n_2}) \times |T^{FRDWBA}|^2, \tag{20}$$

where $v_a$ is the relative velocity of the projectile in the initial channel.

The four-body phase space factor is given by (see Appendix B)

$$\rho(E_b, \Omega_b, E_{n_1}, \Omega_{n_1}, \Omega_{n_2}) = \frac{h^{-9} m_t m_b m_{n_1} m_{n_2} p_b p_{n_1} p_{n_2}}{m_{n_2} + m_t - m_{n_2} \frac{\mathbf{p}_{n_2}\cdot(\mathbf{p}_{tot} - \mathbf{p}_b - \mathbf{p}_{n_1})}{p^2_{n_2}}}, \tag{21}$$

In Eq.(21), $\mathbf{p}_i$'s ($i = t, b, n_1, n_2$) are the momenta appropriate to the frame of interest (i.e. laboratory or c.m.) and $\mathbf{p}_{tot} = \mathbf{p}_t + \mathbf{p}_b + \mathbf{p}_{n_1} + \mathbf{p}_{n_2}$.

### *2.2 Transition amplitude within the adiabatic (AD) model*

The adiabatic model of Coulomb breakup assumes that the important excitations of the projectile nucleus are in the low energy continuum, i.e. the breakup configurations excited by the projectile-target interaction are low energy $b$+$n_1$+$n_2$ relative motion states. This allows the four-body wave function $\Psi_a^{(+)}(\xi_a, \mathbf{R}, \mathbf{r}, \mathbf{r}_i)$ to be written as [40]

$$\Psi_a^{(+)}(\xi_a, \mathbf{R}, \mathbf{r}, \mathbf{r}_i) = \phi_a(\xi_a, \mathbf{R}, \mathbf{r}) e^{i\alpha \mathbf{k}_a\cdot\mathbf{R}} \chi^{(+)}_{a-t}(\mathbf{k}_a, \mathbf{r}_b). \tag{22}$$

The AD model is a non-perturbative theory and it does not make the weak coupling approximation of DWBA. However, the initial and final state Coulomb interactions are included to all orders in both the formalisms. It may be noted that while the AD model necessarily requires the valence nucleons to be chargeless, the FRDWBA can, in principle, be applied to cases where both the core and the valence particles are charged.

The expression for the transition amplitude for the Coulomb breakup of a Borromean nucleus within the adiabatic model is given by [40]

$$\begin{aligned}
T^{AD} = & e^{-\pi(\eta_a+\eta_b)/2}\Gamma(1+i\eta_a)\Gamma(1+i\eta_b) \\
& \times [\int d\mathbf{r}_i e^{i(\mathbf{k}_a-\mathbf{k}_b-\beta\mathbf{k}_c)\cdot\mathbf{r}_b} {}_1F_1(-i\eta_a, 1, i(k_a r_b - \mathbf{k}_a\cdot\mathbf{r}_b)) \\
& \times {}_1F_1(-i\eta_b, 1, i(k_b r_b + \mathbf{k}_b\cdot\mathbf{r}_b))] \\
& \times [\int d\mathbf{r} d\mathbf{R} d\xi e^{-i(\mathbf{k}_c-\alpha\mathbf{k}_a)\cdot\mathbf{R}} e^{-i\mathbf{k}\cdot\mathbf{r}} \phi_b^*(\xi_b)\phi_{n_1n_2}^*(\xi_{12})V(\mathbf{R},\mathbf{r}) \\
& \times \phi_a(\xi_a,\mathbf{R},\mathbf{r})].
\end{aligned} \tag{23}$$

It is evident that except for the form factor, the transition amplitudes within the FRDWBA and AD formalisms are the same. The form factor in the AD case is given by

$$\begin{aligned}
I_f^{AD} = & \int d\mathbf{r} d\mathbf{R} e^{-i(\mathbf{k}_c-\alpha\mathbf{k}_a)\cdot\mathbf{R}} e^{-i\mathbf{k}\cdot\mathbf{r}} [\int d\xi \phi_b^*(\xi_b)\phi_{n_1n_2}^*(\xi_{12})V(\mathbf{R},\mathbf{r}) \\
& \times \phi_a(\xi_a,\mathbf{R},\mathbf{r})].
\end{aligned} \tag{24}$$

It may be noted that Eq. (23) can also be obtained within the DWBA model by making ELMA to the Coulomb distorted wave in the initial channel of the reaction, and by evaluating the local momentum at $R = \infty$ with its direction being the same as that of the projectile.

## 3 Structure models

The three-body wave function for the ground state (g.s.) of $^6$He used in our calculations (which was provided to us by the authors of Ref. [17]) has been obtained [17] by solving the Faddeev equation with the hyperspherical harmonic expansion method which included a maximum of 20 hyperharmonics. In these calculations the $n$-$^4He$ interaction was taken from Ref. [42], and for the $n$-$n$ interaction the Gogny-Pires-Tourreil potential [43] with spin-orbit and tensor components was used. The two-neutron separation energy and root mean square (rms) matter radius of $^6$He predicted by this model were 0.975 MeV and 2.50 fm, respectively. The $\alpha$-particle rms radius was taken to be 1.49 fm.

We would like to emphasize that in this paper our main intention is to develop a post form FRDWBA theory of the Coulomb breakup of the Borromean nuclei where a three-body wave function for their ground state can be used. This enables the breakup observables to be employed as additional constraints on the three-body structure models of these systems. Performing structure calculations is outside the scope of this paper. Nevertheless, it would be worthwhile to use the g.s. wave function of $^6$He calculated by other authors (see eg. [44] where the calculations for the $^6$He have been done within the Faddeev approach using different sets of interactions), to see the sensitivity of our results on the structure models of $^6$He.

For the dineutron model calculations, a point-like 'dineutron' was assumed to be bound to the $^4$He core in a $1s$ state. The corresponding interaction is described by a Woods-Saxon potential (with radius and diffuseness parameters of 1.15 fm and 0.5 fm respectively) whose depth is adjusted to reproduce the binding energy of 0.975 MeV. The resulting $^6$He wave function has the rms radius of 2.47 fm, with the same $\alpha$-particle rms radius as that mentioned above.

## 4 Results and discussions

### 4.1 $\alpha$-particle energy distribution

In Fig. 2, we show a comparison of the calculated and measured $\alpha$-particle energy spectra at $\theta_\alpha = 5^\circ$ in the elastic breakup of $^6$He on a Au target at the beam energy of 63.2 MeV/nucleon. The data are taken from Ref. [45]. These cross sections have been obtained by performing the neutron angular integrations (in Eq. (20)) up to $20^\circ$ and $360^\circ$ in the theta and phi planes, respectively. The results remained almost unaffected by increasing the theta angle further. All the kinematically allowed values were included in the neutron energy integration. The solid, dotted and dashed lines show the results of calculations performed within the FRDWBA, AD and dineutron models respectively. The results of the last model are plotted after multiplying the actual cross sections by the factor shown in the figure. It may be noted that the theoretical spectrum in all the cases is shifted backwards by 10 MeV to compensate for the energy loss due to the target thickness [45,40]. It is seen that the FRDWBA results are about 20% larger than those of the AD model at the $\alpha$ particle energies near and above the peak region. However, both of them are lower than the experimental data. The grazing angle for the reaction studied in this figure is about $3.5^\circ$. Therefore, nuclear breakup effects are expected to make significant contribution to the cross sections at the angle for which these data are taken. This could explain the pure Coulomb breakup results being smaller

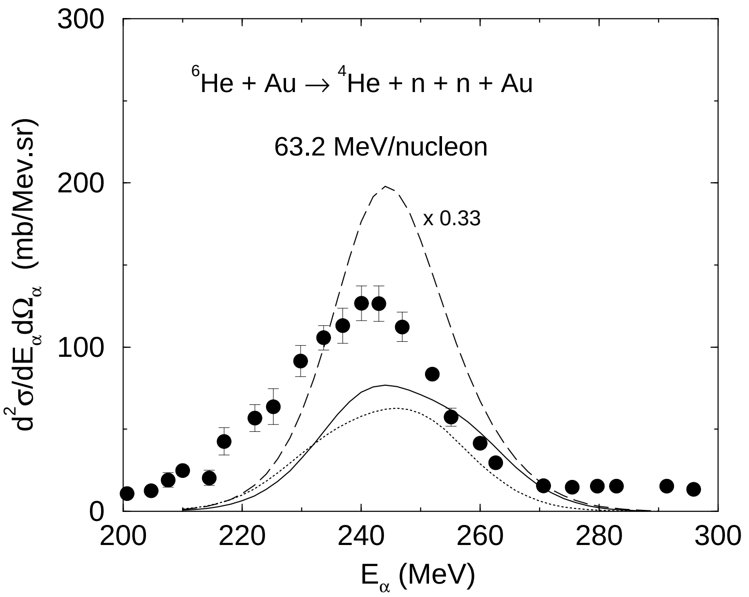

Fig. 2. Calculated energy distributions of $\alpha$-particle in the elastic breakup of $^6$He on a Au target at 63.2 MeV/nucleon at $\theta_\alpha = 5^\circ$. The solid, dotted and dashed curves represent the results of the FRDWBA, AD and dineutron models respectively. The results of the di-neutron model have been plotted after multiplying the actual cross sections by 0.33. The data have been taken from [45].

than the experimental cross sections, particularly in the peak region.

It may be noted that the 'dineutron' model overestimates the measured cross sections by a factor of about 3 (the dashed line). This result can be understood qualitatively by recalling that the magnitudes of the calculated cross sections are dependent on the mean square distance between the $\alpha$-particle and the center of mass of $^6$He [46]. In case of the three-body wave function, this distance is 1.428 fm$^2$, whereas for the 'dineutron' model, it is 2.32 fm$^2$. The larger cross section obtained in the latter model, therefore, may be attributed to this difference.

Measurements performed below the grazing angle are expected to be less affected by the nuclear breakup. One could then hope to test the significance of the small but noticeable difference seen in the pure Coulomb breakup cross sections calculated within the FRDWBA and AD models. However, it can already be seen that the peak position in the cross section calculated within the former is somewhat shifted to smaller energies as compared to that of the latter and is in a slightly better agreement with the peak position of the data.

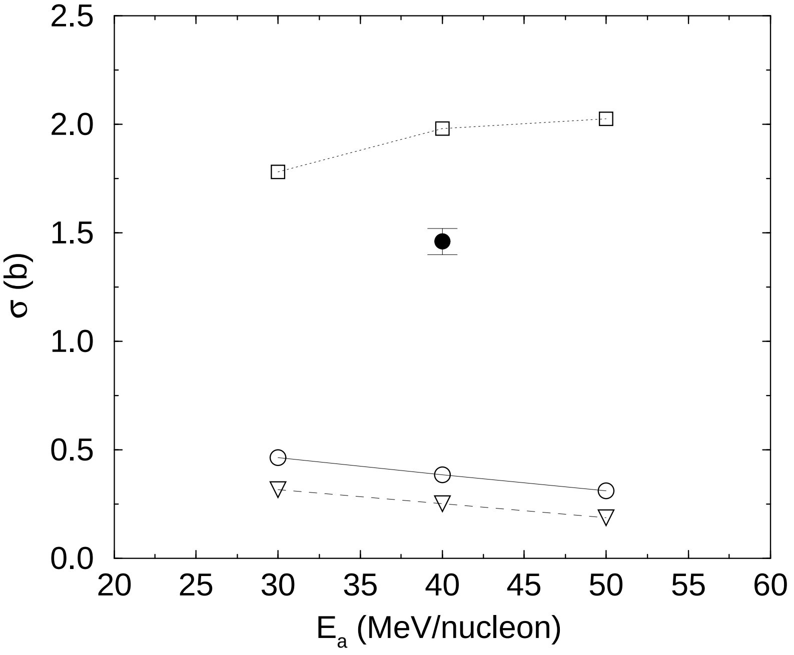

Fig. 3. Calculated Coulomb part of total two-neutron removal cross sections for breakup of $^6$He on a Pb target at three different beam energies of 30, 40 and 50 MeV/nucleon. The open triangles, open circles and open squares show the results of the AD, FRDWBA and dineutron models respectively. The data point is the average of the experimental total two-neutron removal cross sections measured between the beam energies of 28 MeV/nucleon to 52 MeV/nucleon ([47]).

### *4.2 Coulomb part of total two-neutron removal cross sections*

In Fig. 3, we show the results of calculations for the Coulomb part of the total two-neutron removal cross section at three different beam energies of 30, 40 and 50 MeV/nucleon for the breakup reaction of $^6$He on a $^{208}$Pb target. The open circles, open triangles and open squares show the results of the FRDWBA, AD and dineutron models respectively. With increasing beam energy the cross sections of first two models decrease, which is consistent with the earlier observations (see *e.g.* [27]). We note that here also the results of these two models differ from each other by 20-25%, but both of them are smaller than the rough estimates for the pure Coulomb breakup cross sections given in Ref. [47]. However, such estimates are unlikely to be accurate for nuclei having a halo structure as discussed in [48,49].

That the nuclear breakup contributions are substantial in the case of breakup of $^6$He even on a heavy target, is evident from this figure, where we also show (solid circle) the experimental value of the measured total two-neutron removal cross section($\sigma_{-2n}^{exp}$), which is the average of the measurements performed at beam energies between 28 to 52 MeV/nucleon. Our theoretical values correspond only to the Coulomb part of the elastic breakup cross section, while

$\sigma_{-2n}^{exp}$ has contributions from the Coulomb, nuclear as well as their interference terms. Moreover, the nuclear breakup consists also of the inelastic breakup mode [50] (which is called as the stripping process in Ref. [36]). Therefore, to understand the data of Ref. [47], it is essential to calculate the nuclear breakup cross sections on the same footing as the Coulomb one. Similarly, in the breakup of $^6$He on the Pb target at the higher beam energy of 240 MeV/nucleon, the calculated pure Coulomb two-neutron removal cross section is 62.5 mb, which is quite small as compared to the corresponding value of $\sigma_{-2n}^{exp}$ [51]. This difference too can be understood from the fact that the cross sections corresponding to the nuclear elastic and inelastic breakup modes are quite large [33,37].

The pure Coulomb two-neutron removal cross sections, calculated within the dineutron model (open squares), are even larger than $\sigma_{-2n}^{exp}$, and have a wrong type of the beam energy dependence. Thus, the dineutron model is not suitable for describing the data for the breakup of $^6$He.

### *4.3 α-particle momentum distributions*

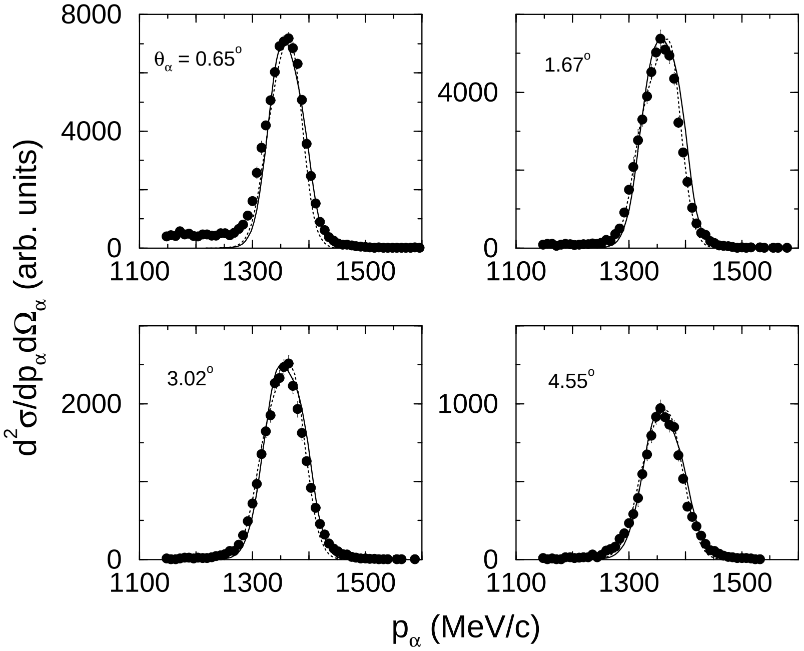

Fig. 4. Comparison of the calculated and measured total momentum distributions of the alpha particle in the breakup of $^6$He on a Au target at 64 MeV/nucleon at four forward angles. The results of the FRDWBA and AD models are shown by the solid and dotted lines, respectively. The data are taken from [52].

In Fig. 4, we compare the calculated and measured [52] total momentum distributions of the $\alpha$-particle emitted in the breakup of $^6$He on the Au target at the beam energy of 64 MeV/nucleon. The $\alpha$-particle was detected at four average angles of 0.65°, 1.67°, 3.02° and 4.55° [52]. In this experiment, the coincident $\gamma$-ray technique was used to identify events in which the target nucleus was simultaneously excited. The elastic breakup events were tagged with $\gamma$-ray multiplicity $M_\gamma = 0$. Since the data are given in arbitrary units, we have normalized our calculations to the peak of the experimental distributions in all four cases. It is clear that shapes of the momentum distributions are well reproduced by our calculations. The full width at half maximum (FWHM) of the momentum distributions changes systematically from 76 MeV/c to 98 MeV/c with increasing angle. This could indicate that the effects related to the reaction dynamics (*e.g.* distortion of the wave functions describing the fragment-target relative motion) lead to the widening of the total momentum distributions as a function of the detection angle.

It should be remarked here that the calculations [53], where the total momentum distributions are obtained from the momentum space wave functions of the ground state of the projectile disregarding the reaction dynamics altogether, are unlikely to describe this feature of the experimental data. At the same time, if the detection angle increases further the nuclear breakup effects will become more important and pure Coulomb breakup may also become inadequate to describe the FWHM of the experimental total momentum distributions. Therefore, it would be interesting to span a larger range of detection angles in future experiments.

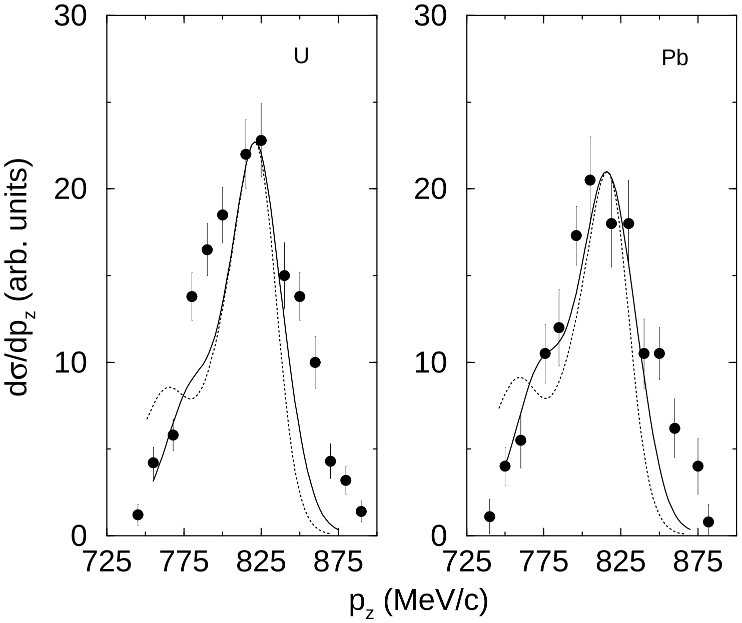

Fig. 5. Parallel momentum distribution of the alpha particle emitted in the Coulomb breakup of $^6$He on U and Pb targets at the beam energy of 24 MeV/nucleon. The FRDWBA and AD model results are shown by the solid and dotted lines respectively. The data are taken from [54].

In Fig. 5, we present the comparison of our calculations with the data for the parallel momentum ($p_z$) distribution of the $\alpha$-particle emitted in the breakup reaction of $^6$He on U and Pb targets at the beam energy of 24 MeV/nucleon. These measurements have recently been performed at the Michigan State University [54]. The calculated distributions have been obtained by integrating Eq. (20) over the neutron angles up to 5.7° (which is the minimum opening angle of the neutron detector in this experiment [54]). The calculated results are normalized to the peak of the data. We note that although both FRD-WBA and AD models are able to reproduce the FWHM of the experimental $p_z$ distributions ($\sim$ 76 MeV/c) reasonably well, the former is in slightly better agreement with the data.

### *4.4 Neutron-neutron and core-neutron relative energy spectra*

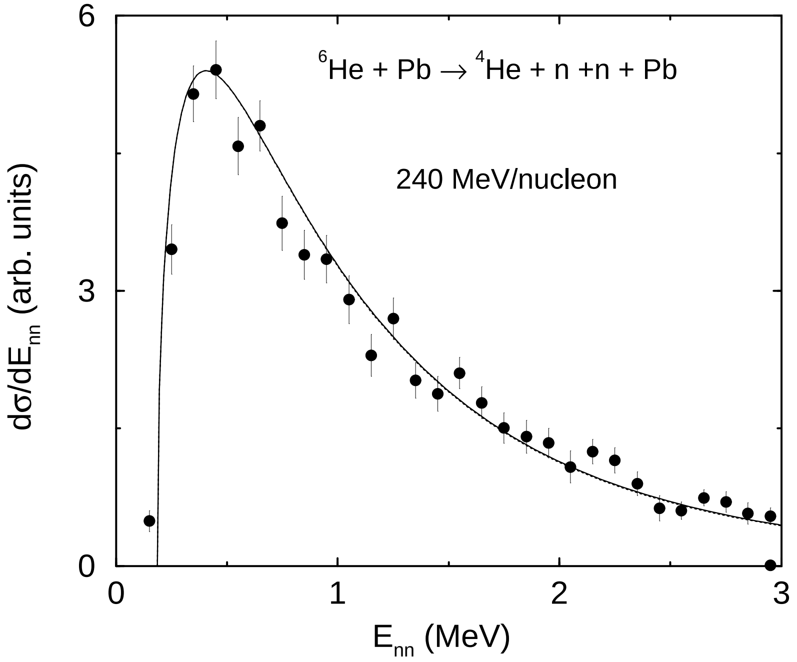

Fig. 6. Calculated neutron-neutron relative energy spectra in the Coulomb breakup of $^6$He on the Pb target at the beam energy of 240 MeV/nucleon. The FRDWBA and adiabatic model results are shown by the solid and dotted lines respectively. The data are taken from [51].

In Fig. 6, we show the comparison of our calculations with the data [51] for the neutron-neutron relative energy ($E_{nn}$) spectrum obtained in the breakup of $^6$He on a Pb target at the beam energy of 240 MeV/nucleon. The calculated spectrum has been obtained by transforming the cross section shown in Eq. (20) to the frame of relative and c.m. motion of the fragments (see Appendix B), and integrating the resultant over the unobserved variables. The integrations over the theta and phi angles of $n_1$-$n_2$ and $\alpha$-($n_1$-$n_2$) systems were carried out in the range of 0°-180° and 0°-360° respectively, while those over the energy $E_{\alpha-(n_1-n_2)}$ are done in the range of 0-10 MeV. However, the integration over the theta angle of the $^6$He-target system ($\theta_{at}$ in Eq. (B.12)) is carried out up to the grazing angle (1.1°) only, as we are interested only in the pure Coulomb contributions to the cross sections. The solid (dotted) line shows the corresponding FRDWBA (AD) model results. Both calculations are normalized to the peak of the experimental data which is at $E_{nn} \sim 0.45$ MeV. Both the models lead to almost similar results which incidently are in good agreement with the shape of the experimental data. Of course, inclusion of the nuclear and Coulomb-nuclear interference terms can affect both the absolute magnitude as well as shape of this distribution. Therefore, it would be interesting to have the data with absolute values on the one hand, and the calculations including both Coulomb and nuclear breakup effects on the other.

The shape of the neutron-neutron energy spectrum reported in Ref. [55] is not in agreement with that of the experimental data. This is due to the fact that these authors have considered a pure sudden approximation, and have ignored the final state interaction effects. This underlines the importance of the reaction dynamics in the breakup reactions even for beam energies around 240 MeV.

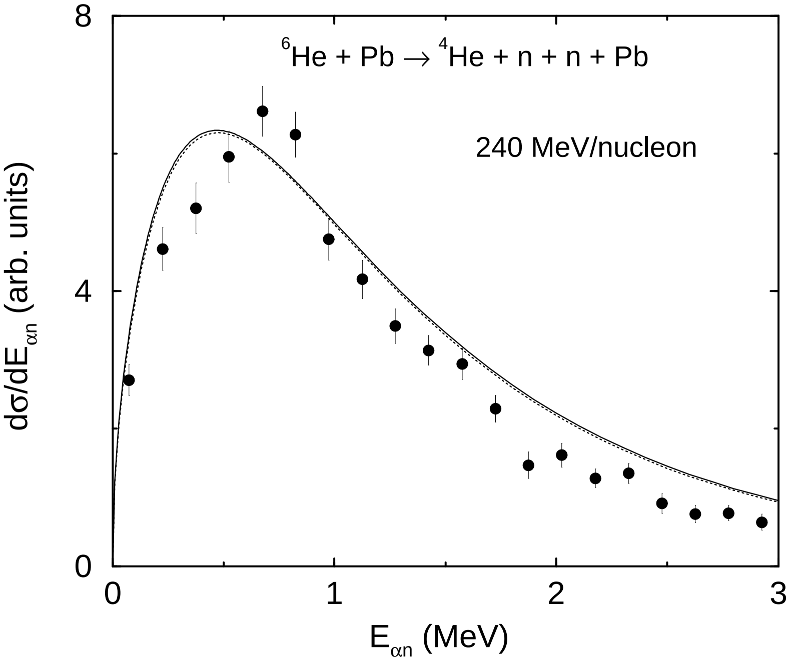

Fig. 7. Calculated $n$-$\alpha$ relative energy spectra in the Coulomb breakup of $^6$He on the Pb target at the beam energy of 240 MeV/nucleon. The FRDWBA and AD model results are shown by the solid and dotted lines respectively. The data are taken from [51].

In Fig. 7, we have compared the calculated $n$-$^4$He relative energy ($E_{\alpha n}$) spectrum with the corresponding experimental data [51]. The peaks of the theoretical calculations are normalized to the maximum of the experimental data. The theoretical cross sections have been obtained by integrating Eq. (B.14) of Appendix B over the unobserved variables. The range of the angular and the energy integrations of various variables were the same as that described above in connection with Fig. 6. We see that except for the peak position, the theoretical calculations reproduce the data reasonably well. The difference in the peak positions of the experimental and theoretical spectra may perhaps be attributed to the fact that the position of the $^5$He resonance is not properly reproduced within the three-body model used in getting the ground state wave function of $^6$He employed in our calculations. We plan to check this point in a future study by using other $^6$He wave functions which may be better in this respect.

### *4.5 Excitation energy spectra*

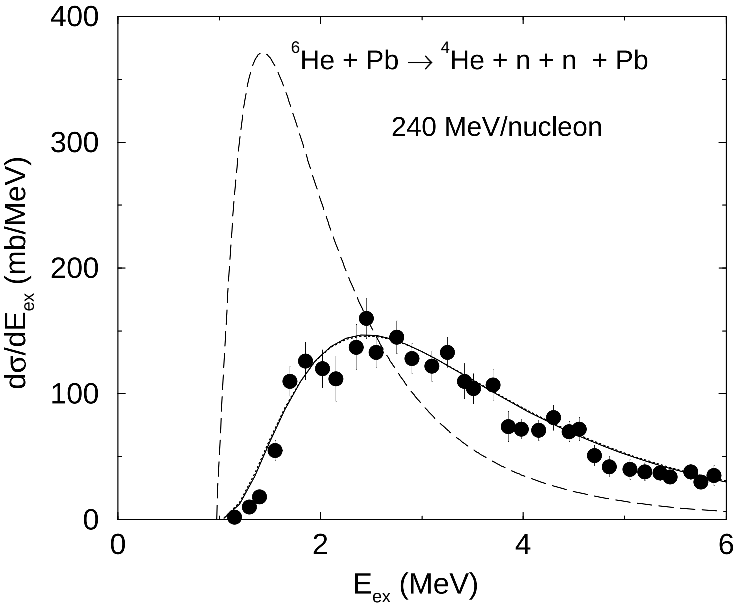

Fig. 8. Calculated excitation energy spectra in the Coulomb breakup of $^6$He on the Pb target at the beam energy of 240 MeV/nucleon. The FRDWBA and AD model results are shown by he solid and dotted lines respectively. The data are taken from [51]. The dashed line shows the result of the dineutron model.

In Fig. 8, we show the pure Coulomb contribution to the excitation energy ($E_{ex}$) spectrum in the breakup of $^6$He on a Pb target at the beam energy of 240 MeV/nucleon [51]. Excitation energy is defined as the sum of the $\alpha$-($n_1$-$n_2$) and $n_1$-$n_2$ relative energies and the $Q$-value of the reaction. The calculated cross sections are normalized to the peak of the data as the elastic Coulomb breakup contribution constitutes only a part of the excitation energy spectrum [37]. We note that both FRDWBA and AD models give identical results and are able to reproduce the shape of the spectrum well. We have also shown in this figure the results obtained with the dineutron model, which is clearly inadequate to describe the data. It should, however, be noted that the calculated cross sections have not been convoluted with the detector response matrix as suggested in [51]. As is shown in [51], this folding reduces the cross sections by about 20 % near the peak region, and by less that 5% beyond it. Therefore, the agreement with the data seen in Fig. 8 should be seen in this context.

## 5 Summary and Conclusions

In this paper we have calculated the elastic Coulomb breakup of the Borromean nucleus $^6$He within a four–body post form distorted wave Born approximation approach. The finite range effects have been included by using an effective local momentum approximation on the Coulomb distorted wave function of the charged heavy core in the outgoing channel. This method allows the use of realistic correlated three-body wave functions for the projectile. Thus the special features associated with the structure of the two-neutron halo systems can be taken into account in the reaction calculations. In our method, the breakup amplitude is expressed as a product of the factors describing separately the projectile structure and the dynamics of the reaction. This feature of our theory is common with that of the adiabatic model of the Coulomb breakup reactions. Although unlike DWBA, this model does not use the weak coupling approximation to describe the center of mass motion of the fragments with respect to the target, yet it leads to results which agree with those of the FRDWBA within approximately 20%. The existing data are unable to highlight the significance of this small difference between the two calculations. Measurements done below the grazing angle may be helpful in this respect.

We have presented calculations for the energy, total and parallel momentum distributions of the $\alpha$-particle as well as for the neutron-neutron and $\alpha$-neutron relative energy spectra. In all the cases, our calculations are able to reproduce the shapes of the experimental spectra reasonably well. However, the absolute magnitudes of the data (wherever available) were underpredicted by both finite range DWBA and adiabatic model of the Coulomb breakup. This suggests that nuclear breakup contributions are substantial in the kinematical regimes covered by these data. Furthermore, although the pure Coulomb calculations are able to reproduce the shapes of the experimental data on the fragment-fragment correlations, inclusion of nuclear breakup effects are necessary for a more comprehensive description of the data. Our calculations rule out the point-like dineutron-core type of models for describing the breakup of Borromean systems. The two-body fragment-fragment correlation data are beyond the scope of such models.

The authors are thankful to Ian Thompson of the University of Surrey for providing them the three-body wave function of $^6$He used in the calculations reported in this paper and to Tom Aumann and Hans Emling of GSI, Darmstadt for making them available in tabular form the experimental data reported in Figs. 6,7, and 8. One of us (RS) wishes to thank Pawel Danielewicz for the kind hospitality of the theory group of the National Superconducting Cyclotron Laboratory of the Michigan State University where this paper was finalized. He also wishes to thank Aaron Galonsky for several useful discussions regarding the experimental data reported in Fig.5 and for going through the manuscript.

## A Validity of the effective local momentum approximation

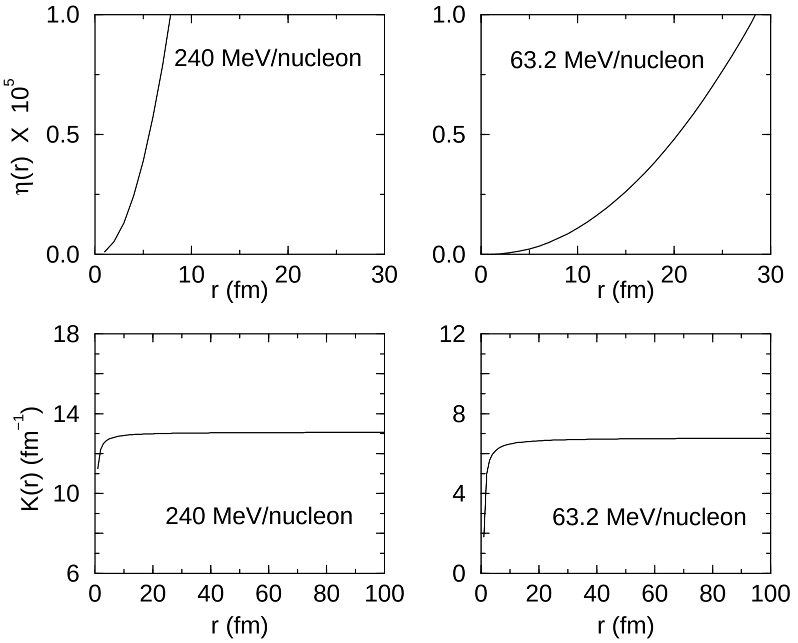

Fig. A.1. Variation of $\eta(r)$ (upper half) and $K(r)$ (lower half) with $r$ for the reaction $^6$He + $^{197}$Au → $^4$He + $n$ + $n$ + $^{197}$Au at the beam energies of 240 MeV/nucleon (left side) and 63.2 MeV/nucleon (right side).

The derivation of the finite range amplitude [Eq. (13)] uses an effective local momentum approximation (ELMA). This allows us to write the distorted wave function of argument $\mathbf{r}_b$ as a product of the plane wave of argument $\mathbf{R}$ and distorted wave of argument $\mathbf{r}_i$. This simplifies the evaluation of the six-dimensional integrals by reducing them as a product of two three-dimensional integrals of independent arguments.

As discussed in [56], a condition for the validity of this approximation is that the quantity

$$\eta(r) = \frac{1}{2}K(r)|dK(r)/dr|^{-1} \tag{A.1}$$

evaluated at a representative distance $R_d$ should be much larger than the rms radius of the projectile. To check this, we show in Fig. A.1, $\eta(r)$ (upper half) and $K(r)$ (the magnitude of the local momentum) (lower half) as a function of $r$, for the breakup reactions $^{6}$He + $^{197}$Au → $^{4}$He + $n$ + $n$ + $^{197}$Au at the beam energies of 240 MeV/nucleon (left side) and 63.2 MeV/nucleon (right side). We see that for $r > 8$ fm, $\eta(r)$ is several orders of magnitude larger than rms radii of the halo in both the cases. Therefore, the above condition is well satisfied.

¿From the lower half of Fig. A.1, we note that the value of $K(r)$ remains constant for distances larger than 10 fm for both the beam energies. Due to the peripheral nature of the breakup reaction, this region contributes maximum to the cross section. Therefore, our choice of a constant magnitude for the local momentum evaluated at 10 fm is well justified and is independent of the beam energy. In fact, we noted that as $R_d$ is increased from 5 to 10 fm the calculated cross sections vary by at the most 10 %, and with a further increase the variation is less than 1 %, in all the cases considered in this paper.

In the application of the ELMA in the description of the heavy ion induced transfer reactions [57] and the breakup reaction of the one-neutron halo nuclei [24], the calculated cross sections were found to be almost unaffected by the choice of the direction of the local momentum. To study the sensitivity of our FRDWBA results on the direction of $\mathbf{K}$ for reactions under study in this paper, we have performed calculations for three cases where we take the angles of the local momentum ($d_1$) parallel to those of $\mathbf{k}_b$, ($d_2$) parallel to the direction corresponding to the half of the angles of $\mathbf{k}_b$ and ($d_3$) parallel to the beam direction (zero angles). In the upper part of Fig. A.2, we show the energy distribution of the alpha particle for the same reaction as described in Fig. 2. The results obtained with cases $d_1$, $d_2$ and $d_3$ are shown by solid, dashed and dotted lines respectively. We note that energy distributions calculated with these choices are almost identical. The results for the neutron-neutron energy correlations for the same reaction as in Fig. 6, are shown in the lower part of this figure for the choices ($d_1$), ($d_2$) and ($d_3$) for the direction of the local momentum. In this case too we observe almost no variation in the calculated cross sections. Similarly, we have noted no dependence of the calculated widths of the parallel momentum distributions of heavy fragments on the direction of $\mathbf{K}$, in all the reactions investigated in this paper. Therefore, the dependence of various cross sections for the reactions studied in this paper, on the direction of the local momentum is either very minor or almost negligible. The mea-

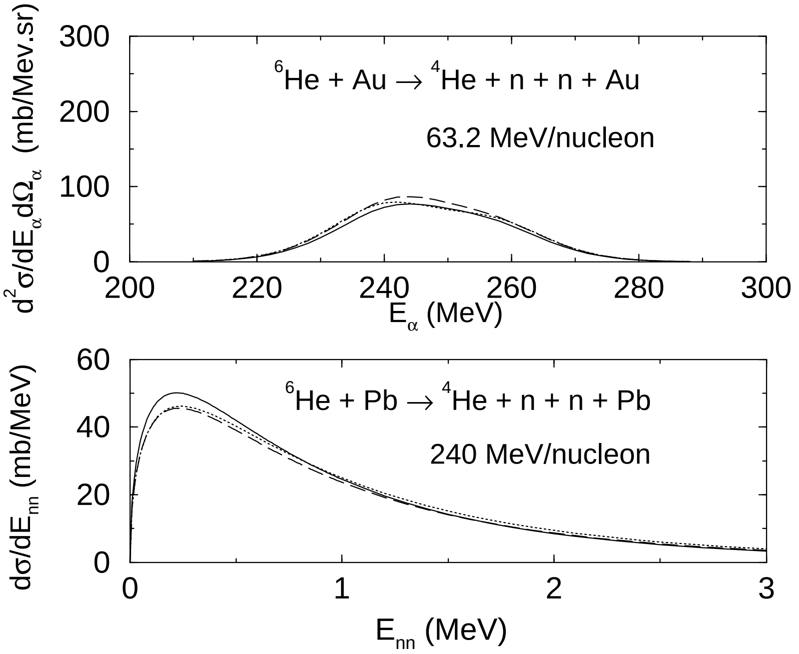

Fig. A.2. The energy distributions of the alpha particle in the reaction $^6$He + $^{197}$Au → $^4$He + $n$ + $n$ + $^{197}$Au at the beam energy of 63.2 MeV/nucleon (upper part), and the neutron-neutron energy correlation in the reaction $^6$He + $^{208}$Pb → $^4$He + $n$ + $n$ + $^{208}$Pb at the beam energy of 240 MeV/nucleon (lower part), for choices $d_1$ (solid line), $d_2$ (dashed line) and $d_3$ (dotted line) for the direction of the local momentum, as discussed in the text.

surements done so far are not able to distinguish the small differences that we see here in some cases. Hence, we have performed all our calculations in this paper by using the direction of the momentum $\mathbf{K}$ to be the same as that of $\mathbf{k}_b$.

## B The four – body phase space factor for a given Q value

The phase space in which we fix the total energy $E_{tot}$ in the final state at the value $E$ is given by

$$d\sigma = h^{-9}\delta(E_{tot} - E)d\mathbf{p}_b d\mathbf{p}_{n_1} d\mathbf{p}_{n_2} \tag{B.1}$$

The total energy is given by

$$\begin{aligned} E_{tot} &= E_a + Q \qquad &\text{(B.2)}\\ &= E_t + E_b + E_{n_1} + E_{n_2} \qquad &\text{(B.3)} \end{aligned}$$

$$
\begin{aligned}
&= E_b + E_{n_1} + \frac{p_{n_2}^2}{2m_{n_2}} + \frac{p_t^2}{2m_t} && \text{(B.4)}\\
&= E_b + E_{n_1} + \frac{p_{n_2}^2}{2m_{n_2}} + \frac{1}{2m_t}[(\mathbf{p}_{tot} - \mathbf{p}_b - \mathbf{p}_{n_1})^2 + p_{n_2}^2 && \text{(B.5)}\\
&- 2\mathbf{p}_{n_2}.(\mathbf{p}_{tot} - \mathbf{p}_b - \mathbf{p}_{n_1})],
\end{aligned}
$$

where $E_a$ is the projectile energy and $Q$ is the Q-value of the reaction (<0). $\mathbf{p_{tot}}$ is the total momentum of the projectile in the incident channel, which by momentum conservation, is given by

$$
\mathbf{p}_{tot} = \mathbf{p}_t + \mathbf{p}_b + \mathbf{p}_{n_1} + \mathbf{p}_{n_2}. \tag{B.6}
$$

Using $d\mathbf{p} = m.p.dE.d\Omega$, we have

$$
\begin{aligned}
\frac{d\sigma}{dE_b d\Omega_b dE_{n_1} d\Omega_{n_1} dE_{n_2} d\Omega_{n_2}} &= m_b p_b m_{n_1} p_{n_1} m_{n_2} p_{n_2} \frac{d\sigma}{d\mathbf{p}_b d\mathbf{p}_{n_1} d\mathbf{p}_{n_2}} && \text{(B.7)}\\
&= h^{-9} \delta(E_{tot} - E) m_b p_b m_{n_1} p_{n_1} m_{n_2} p_{n_2} && \text{(B.8)}
\end{aligned}
$$

Therefore

$$
\begin{aligned}
\rho(E_b, \Omega_b, E_{n_1}, \Omega_{n_1}, \Omega_{n_2}) &= \frac{d\sigma}{dE_b d\Omega_b dE_{n_1} d\Omega_{n_1} d\Omega_{n_2}}\\
&= \int \frac{d\sigma}{dE_b d\Omega_b dE_{n_1} d\Omega_{n_1} dE_{n_2} d\Omega_{n_2}} dE_{n_2}\\
&= h^{-9} m_b m_{n_1} m_{n_2} \int p_b p_{n_1} p_{n_2} \delta(E_{tot} - E) dE_{n_2}\\
&= h^{-9} m_b m_{n_1} m_{n_2} \Big[\frac{p_b p_{n_1} p_{n_2}}{\partial E_{tot}/\partial E_{n_2}}\Big]_{E_{tot}=E} && \text{(B.9)}
\end{aligned}
$$

Now from Eq.(B.5)

$$
\frac{\partial E_{tot}}{\partial E_{n_2}} = \frac{\partial E_{tot}}{\partial p_{n_2}} \frac{dp_{n_2}}{dE_{n_2}} = \frac{1}{m_t}[m_{n_2} + m_t - m_{n_2} \frac{\mathbf{p}_{n_2}.(\mathbf{p}_{tot} - \mathbf{p}_b - \mathbf{p}_{n_1})}{p_{n_2}^2}] \tag{B.10}
$$

Therefore

$$
\rho(E_b, \Omega_b, E_{n_1}, \Omega_{n_1}, \Omega_{n_2}) = \frac{h^{-9} m_t m_b m_{n_1} m_{n_2} p_b p_{n_1} p_{n_2}}{m_{n_2} + m_t - m_{n_2} \frac{\mathbf{p}_{n_2}.(\mathbf{p}_{tot} - \mathbf{p}_b - \mathbf{p}_{n_1})}{p_{n_2}^2}}. \tag{B.11}
$$

It can also be shown that

$$\frac{d^5\sigma}{dE_{n_1n_2}d\Omega_{n_1n_2}dE_{b-(n_1n_2)}d\Omega_{b-(n_1n_2)}d\Omega_{at}} = J_1 \times \frac{d^5\sigma}{dE_b d\Omega_b dE_{n_1} d\Omega_{n_1} d\Omega_{n_2}}, \tag{B.12}$$

where

$$J_1 = \frac{m_{n_1n_2}p_{n_1n_2}m_{b-(n_1n_2)}p_{\alpha-(n_1n_2)}m_{at}p_{at}}{h^9\rho(E_b, \Omega_b, E_{n_1}, \Omega_{n_1}, \Omega_{n_2})} \tag{B.13}$$

and

$$\frac{d^5\sigma}{dE_{bn_1}d\Omega_{bn_1}dE_{n_2-(bn_1)}d\Omega_{n_2-(bn_1)}d\Omega_{at}} = J_2 \times \frac{d^5\sigma}{dE_b d\Omega_b dE_{n_1} d\Omega_{n_1} d\Omega_{n_2}}, \tag{B.14}$$

where

$$J_2 = \frac{m_{bn_1}p_{bn_1}m_{n_2-(bn_1)}p_{n_2-(bn_1)}m_{at}p_{at}}{h^9\rho(E_b, \Omega_b, E_{n_1}, \Omega_{n_1}, \Omega_{n_2})}. \tag{B.15}$$

## References

[1] I. Tanihata, J. Phys. G 22 (1996) 157.

[2] P. G. Hansen, A. S. Jensen, B. Jonson, Annu. Rev. Nucl. Part. Sci. 45 (1995) 591.

[3] M. V. Zhukov, B. V. Danilin, D. V. Fedorov, J. M. Bang, I. J. Thompson, J. S. Vaagen, Phys. Rep. 231 (1993) 151; and references therein.

[4] P. G. Hansen, B. Jonson, Europhys. Lett. 4 (1987) 409.

[5] I. Tanihata et al., Phys. Lett. B. 160 (1985) 380.

[6] D. V. Fedorov, A. S. Jensen, K. Riisagar, Phys. Rev. C 50 (1994) 2372.

[7] V. Efimov, Comments Nucl. Part. Phys. 19 (1990) 271.

[8] D. R. Lehman, W.C. Parke, Phys. Rev. C 28 (1983) 364; W. C. Parke, D. R. Lehman, Phys. Rev. C 29 (1984) 2319; A. Eskandarian, D.R. Lehman, W.C. Parke, Phys. Rev. C 39 (1989) 1685.

[9] Y. Suzuki, Nucl. Phys. A 528 (1991) 395.

[10] J. M. Bang, L. S. Ferreira, E. Maglione, Europhys Lett. 18 (1992) 679.

[11] B. V. Danilin, M. V. Zhukov, J. S. Vaagen, J. M. Bang, Phys. Lett. B 302 (1993) 129.

[12] A. Csótó, Phys. Rev. C 48 (1993) 165; *ibid* Phys. Rev. C 49 (1994) 3035.

[13] S. Funada, H. Kameyama, Y. Sakuragi, Nucl. Phys. A 575 (1994) 93.

[14] B. V. Danilin, I. J. Thompson, M. V. Zhukov, J. S. Vaagen, J. M. Bang, Phys. Lett. B 333 (1994) 299.

[15] S. Aoyama, Shigeo Mukai, K. Kato, K. Ikeda, Prog. Theo. Phys. 53 (1995) 99; *ibid* Prog. Theo. Phys. **94** (1995) 343.

[16] B. V. Danilin, T. Rogde, S. N. Ershov, H. Heiberg-Andersen, J. S. Vaagen, I. J. Thompson, M. V. Zhukov, Phys. Rev. C 55 (1997) R577.

[17] B. V. Danilin, I. J. Thompson, M. V. Zhukov, J. S. Vaagen, Nucl. Phys. A 632 (1998) 383.

[18] S. N. Ershov, T. Rodge, B. V. Danilin, J. S. Vaagen, I. J. Thompson, F. A. Gareev, Phys. Rev. C 56 (1997) 1483.

[19] I. J. Thompson, B. V. Danilin, V. D. Efros, M. V. Zhukov, J. S. Vaagen, J. Phys. G 24 (1998) 1505.

[20] J. M. G. Gomez, C. Prieto, A. Poves, Phys. Lett. B 295 (1992) 1.

[21] W. Koepf, Y. K. Gambhir, P. Ring, M. M. Sharma, Z. Phys. A 340 (1991)119.

[22] Z. Y. Zhu et al., Phys. Lett. B 328 (1994) 1.

[23] B. Pudliner, V. R. Pandaripande, J. Carlson, S.C. Pieper, R.B. Wiringa, Phys. Rev. C 56 (1997) 1720.

[24] R. Chatterjee, P. Banerjee, R. Shyam, Nucl. Phys. A 675 (2000) 477.

[25] S. Nakayama et al., Phys. Rev. Lett. 85 (2000) 262.

[26] L. F. Canto, R. Donangelo, A. Romanelli, H. Schulz, Phys. Lett. B 318 (1993) 415.

[27] P. Banerjee, R. Shyam, Nucl. Phys. A 561 (1993) 112; R. Shyam, P. Banerjee, G. Baur, Nucl. Phys. A 540 (1992) 341.

[28] C. A. Bertulani, G. Baur, M. S. Hussein, Nucl. Phys. A 526 (1991) 751.

[29] G. Baur, K. Hencken, D. Trautmann, S. Typel, H. H. Wolter, LANL preprint nucl-th/0008033.

[30] E. Garrido, D,V. Fedorov, A.S. Jensen, Nucl. Phys. A 617 (1997) 153.

[31] E. Garrido, D.V. Fedorov and A.S. Jensen, Europhys. Lett. 43 (1998) 386.

[32] E. Garrido, D.V. Fedorov, A.S. Jensen, Europhys. Lett. 50 (2000) 735.

[33] E. Garrido, D.V. Fedorov, A.S. Jensen, Phys. Lett. B 480 (2000) 32.

[34] E. Garrido, D.V. Fedorov, A.S. Jensen, Phys. Rev. C 55 (1997) 1327.

[35] E. Garrido, D.V. Fedorov, A.S. Jensen, Phys. Rev. C 59 (1999) 1272.

[36] G. F. Bertsch, K. Hencken, H. Esbensen, Phys. Rev. C 57 (1998) 1366.

[37] S. N. Ershov, B. V. Danilin, J. S. Vaagen, Phys. Rev. C 62 (2000) 041001(R).

[38] J. A. Tostevin et al., Phys. Lett. B 424 (1998) 219: J.A. Tostevin, S. Rugmai, R.C. Johnson, Phys. Rev. C 57 (1998) 3225.

[39] A. Nordsieck, Phys. Rev. **93** (1954) 785.

[40] P. Banerjee, J. A. Tostevin, I. J. Thompson, Phys. Rev. C 58 (1998) 1337.

[41] J. S. Al-Khalili, I. J. Thompson, J. A. Tostevin, Nucl. Phys. A 581 (1995) 331.

[42] J. Bang, C. Gignoux, Nucl. Phys. A 313 (1979) 119.

[43] D. Gogny, P. Pires, R. de Tourreil, Phys. Lett. B 32 (1970) 591.

[44] A. Cobis, D.V. Fedorov, A.S. Jensen, Phys. Rev. Lett. 79 (1997) 2411; *ibid* Phys. Rev. C 58 (1998) 1403.

[45] D. P. Balamuth et al., Phys. Rev. Lett. 72 (1994) 2355.

[46] Y. Sakuragi, S. Funada, Y. Hirabayashi, Nucl. Phys. A 588 (1995) 65c.

[47] R. E. Warner et al., Phys. Rev. C 62 (2000) 024608.

[48] P. Banerjee, R. Shyam, Phys. Rev. C 61 (1999) 047301.

[49] C. H. Dasso, S. M. Lenzi, A. Vitturi, Nucl. Phys. A 639 (1998) 635.

[50] R. Shyam and H. Lenske, Phys. Rev. C 57 (1998) 2427.

[51] T. Aumann et al., Phys. Rev. C 59 (1999) 1252.

[52] J. E. Bush (University of Pennsylvania, USA), contributions to the Meeting of the American Physical Society, Bloomington, Indiana, 25 - 28 October, 1995 and private communications (1998).

[53] M. V. Zhukov, L. V. Chulkov, B. V. Danilin, A. A. Korsheninnikov, Nucl. Phys. A 533 (1991) 428.

[54] Aaron Galonsky, private communications.

[55] C. Forssén, B. Jonson, M. V. Zhukov, Nucl. Phys. A 673 (2000) 143.

[56] R. Shyam and M. A. Nagarajan, Ann. Phys. (NY) 163 (1985) 285.

[57] P. Braun-Munzinger, H. L. Harney, S. Wenneis, Nucl. Phys. A 236 (1974) 190.